Supplementary Information

Nanoparticles traversing extracellular matrix induce biophysical perturbation of fibronectin depicted by surface chemistry

Xing Guo,[a,b] Lin Yang,[a] Chaofan Deng,[a] Luyao Ren,[a] Shixin Li,[c] Xianren Zhang,[d] Jian Zhao[a] and Tongtao Yue*[a]

[a]*Institute of Coastal Environmental Pollution Control, Key Laboratory of Marine Environment and Ecology, Ministry of Education, Ocean University of China, Qingdao, Shandong Province, 266100, China. E-mail: yuetongtao@ouc.edu.cn*

[b]*Guangdong Provincial Key Laboratory of Environmental Pollution and Health, School of Environment, Jinan University, Guangzhou, 511443, China*

[c]*Joint International Research Laboratory of Agriculture and Agri-product Safety of the Ministry of Education, Yangzhou University, Yangzhou 225009, China*

[d]*State Key Laboratory of Organic-Inorganic Composites, Beijing University of Chemical Technology, Beijing 100029, China*

Table S1. List of MD simulations conducted in this work.

Simulation systems	Components	Simulation box size (nm^3)	Simulation time (ns)
Unbiased MD simulations (Protein monomer)	$Fn\text{-}III_{7\text{-}10}$	20 × 20 × 20	200
	$Fn\text{-}III_{7B89}$		
	$NP\text{-}CH_3$ & $Fn\text{-}III_{7\text{-}10}$		
	NP-OH & $Fn\text{-}III_{7\text{-}10}$		
	$NP\text{-}COO^-$ & $Fn\text{-}III_{7\text{-}10}$		
	$NP\text{-}NH_3^+$ & $Fn\text{-}III_{7\text{-}10}$		300
	$NP\text{-}CH_3$ & $Fn\text{-}III_{7B89}$		200
	NP-OH & $Fn\text{-}III_{7B89}$		
	$NP\text{-}COO^-$ & $Fn\text{-}III_{7B89}$		
	$NP\text{-}NH_3^+$ & $Fn\text{-}III_{7B89}$		
Unbiased MD simulations ($Fn\text{-}III_{7B89}$ head-to-tail dimer)	Dimer	20 × 9 × 7	100
	$NP\text{-}CH_3$ & Dimer	20 × 20 × 20	200
	NP-OH & Dimer		
	$NP\text{-}COO^-$ & Dimer		
	$NP\text{-}NH_3^+$ & Dimer		
Steered MD simulations	$Fn\text{-}III_{7\text{-}10}$	9.414 × 6.701 × 40	100
	$Fn\text{-}III_{7B89}$	40 × 8.874 × 11.466	
	$NP\text{-}CH_3$ & $Fn\text{-}III_{7\text{-}10}$	40 × 11 × 15	
	NP-OH & $Fn\text{-}III_{7\text{-}10}$	13.5 × 12.5 × 40	
	$NP\text{-}COO^-$ & $Fn\text{-}III_{7\text{-}10}$	40 × 12 × 12	
	$NP\text{-}NH_3^+$ & $Fn\text{-}III_{7\text{-}10}$	15 × 40 × 13	
	$NP\text{-}CH_3$ & $Fn\text{-}III_{7B89}$	40 × 9.493 × 11.694	
	NP-OH & $Fn\text{-}III_{7B89}$	8.791 × 40 × 11.225	
	$NP\text{-}COO^-$ & $Fn\text{-}III_{7B89}$	40 × 13.09 × 14.64	
	$NP\text{-}NH_3^+$ & $Fn\text{-}III_{7B89}$	40 × 12.147 × 12.216	

Table S2. Top 20 sites of NP-CH_3 binding to Fn-III_{7-10} predicted by molecular docking.

No.	Docking score	Residue Number
1 (Site 1)	-3.7945	1173 1174 1175 1193 1194 1195 1219
2 (Site 2)	-3.7302	1340 1341 1387 1389 1418 1491 1498
3	-3.6961	1173 1174 1175 1176 1193 1194 1195 1219
4	-3.6690	1148 1150 1163 1164 1165 1199 1200
5	-3.5286	1253 1289 1290 1291
6	-3.4899	1258 1259 1260 1261 1262 1264 1287 1288
7	-3.4161	1398 1405 1406 1407 1408
8	-3.3582	1151 1152 1153 1232 1233 1235
9	-3.3386	1151 1152 1153 1232 1233 1235
10	-3.2903	1245 1246 1253 1255 1290
11	-3.2420	1422 1423 1503 1504 1505
12	-3.2038	1176 1217 1224 1225 1226 1227
13	-3.2024	1258 1262 1263 1264 1287 1288
14	-3.1908	1404 1405 1406 1407
15	-3.1464	1332 1333 1409 1410
16	-3.0900	1245 1246 1253 1255
17	-3.0740	1217 1224 1225 1227
18	-3.0597	1151 1152 1153 1232
19	-3.0247	1189 1190 1191
20	-2.9745	1190 1191 1193

Table S3. Top 20 sites of NP-OH binding to Fn-III$_{7\text{-}10}$ predicted by molecular docking.

No.	Docking score	Residue Number
1 (Site 1)	-3.6892	1148 1150 1164 1165 1166 1199
2 (Site 2)	-3.6863	1157 1206 1207 1208 1237 1260 1261
3	-3.6787	1422 1424 1426 1436 1437 1438
4	-3.5677	1157 1206 1208 1237 1260 1261
5	-3.5447	1350 1351 1352 1353 1354 1377
6	-3.4150	1340 1341 1389 1418 1491 1498 1499
7	-3.3783	1258 1259 1260 1261 1262 1264 1287 1288
8	-3.3039	1151 1152 1153 1232 1233 1235
9	-3.2881	1350 1351 1352 1353 1354 1377
10	-3.2821	1258 1259 1260 1261 1262 1264 1267 1287 1288
11	-3.2796	1186 1187 1207 1208 1210 1261 1262
12	-3.2751	1151 1152 1153 1155 1232 1235
13	-3.2408	1245 1246 1253 1255 1290
14	-3.2372	1176 1217 1224 1225
15	-3.1658	1176 1217 1224 1225 1226 1227
16	-3.1030	1422 1424 1436 1437 1438
17	-3.1013	1502 1503 1504
18	-3.0345	1176 1217 1224 1225
19	-3.0087	1176 1217 1224 1225 1226 1227
20	-2.9667	1152 1161 1163 1200

Table S4. Top 20 sites of NP-COO^- binding to Fn-III_{7-10} predicted by molecular docking.

No.	Docking score	Residue Number
1 (Site 1)	-3.5938	1351 1352 1353
2 (Site 2)	-3.5181	1415 1416 1417 1421
3	-3.4884	1324 1401 1403
4	-3.4562	1301 1351 1353
5	-3.3873	1351 1352 1353
6	-3.3241	1270 1280 1304 1306 1320
7	-3.3127	1351 1352 1353
8	-3.3081	1431 1476 1477 1478 1479
9	-3.3025	1142 1143 1144 1145 1224 1225 1226
10	-3.2862	1351 1353
11	-3.2369	1358 1369 1372 1374
12	-3.1910	1446 1448 1488 1490 1497 1499
13	-3.1908	1173 1174 1175 1176 1193 1194 1219
14	-3.1900	1341 1389 1418 1499 1501
15	-3.1555	1350 1351 1352 1353 1354 1377
16	-3.1512	1341 1386 1387 1388 1389
17	-3.1419	1246 1253 1255
18	-3.1379	1243 1245 1253 1255 1290 1291
19	-3.1334	1148 1164 1165 1166 1199
20	-3.1304	1148 1150 1163 1164 1165 1199 1200

Table S5. Top 20 sites of NP-NH_3^+ binding to Fn-$III_{7\text{-}10}$ predicted by molecular docking.

No.	Docking score	Residue Number
1 (Site 1)	-3.8489	1271 1273 1279 1280 1281 1295 1296 1297 1303
2 (Site 2)	-3.6558	1148 1150 1163 1164 1165 1199
3	-3.6230	1148 1150 1163 1164 1165 1199 1200
4	-3.5767	1271 1273 1279 1280 1281
5	-3.5708	1361 1371 1372 1373 1384 1385
6	-3.5462	1271 1279 1280 1281 1295 1296 1297
7	-3.5227	1452 1453 1456 1457 1458 1460
8	-3.5067	1452 1453 1458 1459 1461 1483
9	-3.4608	1148 1150 1163 1164 1165 1166 1199
10	-3.4477	1360 1362 1394 1396 1408 1410
11	-3.4306	1452 1453 1461 1481 1483
12	-3.4148	1178 1179 1180 1189 1190 1191
13	-3.4141	1217 1224 1225 1226
14	-3.4125	1163 1164 1165 1199 1200
15	-3.4047	1360 1362 1370 1394 1396 1410
16	-3.3830	1156 1238 1239 1317 1318 1319
17	-3.3333	1329 1330 1331 1408 1409 1410
18	-3.2993	1156 1238 1239 1318 1319 1320
19	-3.2934	1363 1364 1365 1390 1391
20	-3.2893	1275 1300 1301 1302 1351 1353

Table S6. Top 20 sites of NP-CH_3 binding to Fn-III_{7B89} predicted by molecular docking.

No.	Docking score	Residue Number
1 (Site 1)	-3.9412	1186 1187 1266 1268 1269 1271 1290
2 (Site 2)	-3.8162	1280 1281 1327 1328 1329 1330 1359 1381 1382
3	-3.7803	1197 1198 1200 1201 1203 1206 1227 1228
4	-3.7472	1186 1187 1266 1268 1269 1271 1290
5	-3.7205	1197 1198 1199 1200 1201 1203 1206 1227
6	-3.6165	1304 1307 1308 1311 1329 1332 1334
7	-3.5650	1485 1488 1491 1493 1508 1510 1515
8	-3.5471	1304 1307 1308 1311 1327 1328 1329 1332 1334
9	-3.5333	1187 1188 1290 1291 1292
10	-3.4683	1485 1488 1491 1493 1508 1509 1510 1515
11	-3.4352	1360 1361 1362 1363 1440 1441 1442
12	-3.4011	1238 1239 1294 1342 1343
13	-3.3945	1273 1274 1275 1352 1353 1354
14	-3.3744	1235 1236 1237 1238 1292 1293 1294
15	-3.3601	1279 1280 1360 1362 1381 1382
16	-3.2792	1316 1322 1323 1324
17	-3.1890	1289 1291 1319
18	-3.1510	1388 1390 1392 1404 1406 1432
19	-3.1437	1475 1476 1477 1499 1523
20	-3.1345	1322 1323 1324

Table S7. Top 20 sites of NP-OH binding to Fn-III$_{7B89}$ predicted by molecular docking.

No.	Docking score	Residue Number
1 (Site 1)	-3.6950	1280 1281 1359 1360 1361 1362 1380 1381 1382
2 (Site 2)	-3.6793	1186 1187 1268 1290 1291 1292
3	-3.6307	1197 1198 1200 1201 1203 1206 1227
4	-3.6104	1276 1277 1284 1285 1286 1322 1323 1324
5	-3.5619	1236 1237 1238 1239 1294 1342 1343
6	-3.5225	1238 1239 1293 1294 1342 1343
7	-3.5134	1186 1187 1268 1289 1290 1291 1292
8	-3.4675	1188 1189 1235 1236 1237 1292 1293 1294
9	-3.4617	1304 1308 1311 1329 1332 1334
10	-3.4390	1197 1198 1200 1201 1203 1206 1227
11	-3.4287	1280 1360 1362 1380 1381 1382
12	-3.2795	1187 1290 1291 1292
13	-3.2493	1273 1274 1275 1352 1353
14	-3.2005	1289 1291 1318 1319 1320 1321 1322
15	-3.1514	1316 1320 1322 1323 1324
16	-3.1199	1475 1476 1477 1499 1523
17	-3.0907	1475 1476 1477 1499 1523
18	-3.0476	1288 1289 1291 1322
19	-3.0449	1280 1281 1362 1380 1381 1382
20	-3.0132	1299 1339 1346 1349

Table S8. Top 20 sites of NP-COO$^-$ binding to Fn-III$_{7B89}$ predicted by molecular docking.

No.	Docking score	Residue Number
1 (Site 1)	-3.8907	1396 1397 1422 1423 1424 1446
2 (Site 2)	-3.2142	1393 1395 1401 1403 1417 1418 1419 1420 1425
3	-3.2033	1289 1290 1291 1318 1319 1320
4	-3.1848	1188 1291 1292 1293
5	-3.1291	1393 1395 1401 1403 1417 1418 1425
6	-3.1531	1189 1235 1292 1293 1294
7	-3.1507	1483 1485 1491 1493 1508 1510 1515
8	-3.1071	1393 1395 1403 1417 1418 1419 1420 1425
9	-3.1066	1173 1174 1255 1256 1257
10	-3.0536	1236 1237 1238 1293 1294
11	-3.0389	1371 1419 1421 1450 1473
12	-3.0316	1484 1485 1488 1491 1492 1493 1508 1510 1515
13	-3.0108	1371 1421 1450 1451 1473
14	-2.9838	1475 1476 1477 1499 1523
15	-2.9705	1276 1277 1284 1285 1286 1322 1323 1324
16	-2.9649	1276 1277 1284 1285 1286 1322 1323 1324
17	-2.9605	1304 1306 1307 1308 1311 1329 1332 1334
18	-2.9538	1274 1275 1352
19	-2.9146	1304 1306 1307 1308 1311 1327 1329 1332 1334
20	-2.9132	1280 1281 1327 1328 1330 1359 1381 1382 1384

Table S9. Top 20 sites of NP-NH_3^+ binding to Fn-III_{7B89} predicted by molecular docking.

No.	Docking score	Residue Number
1 (Site 1)	-3.8522	1187 1269 1270 1271 1272 1288 1290
2 (Site 2)	-3.8092	1280 1281 1328 1329 1330 1359 1382 1384
3	-3.6760	1304 1305 1306 1307 1308 1309
4	-3.6644	1360 1361 1362 1439 1440 1441
5	-3.6577	1280 1281 1328 1329 1330 1382
6	-3.6533	1280 1281 1359 1360 1362 1381 1382
7	-3.6329	1186 1187 1266 1269 1271 1290
8	-3.6013	1483 1484 1485 1491 1493 1508 1509 1510 1515
9	-3.5947	1483 1484 1485 1488 1491 1492 1493
10	-3.5207	1274 1275 1352 1353 1354
11	-3.4994	1280 1359 1360 1362 1380 1381 1382
12	-3.4559	1186 1187 1268 1289 1290 1291
13	-3.4526	1280 1359 1360 1362 1381 1382
14	-3.4449	1273 1274 1275 1352 1353 1354
15	-3.4408	1372 1419 1421 1450 1451 1453 1473
16	-3.4301	1276 1277 1284 1285 1286 1322 1323 1324
17	-3.4224	1276 1277 1284 1285 1322 1323 1324
18	-3.3959	1280 1359 1360 1362 1381 1382
19	-3.3939	1312 1314 1323 1324
20	-3.3800	1372 1419 1421 1450 1451 1453 1473

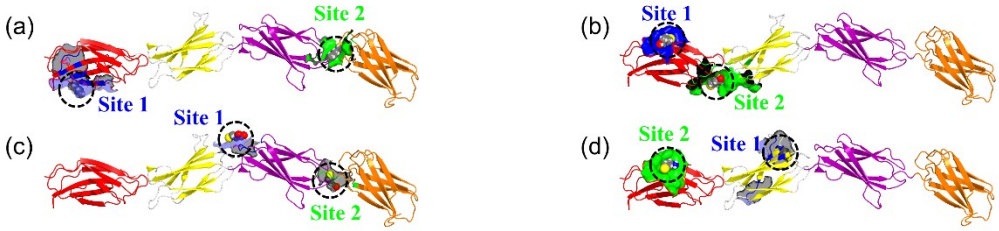

Mode	NP-CH_3	NP-OH	NP-COO^-	NP-NH_3^+
Site 1	-3.7945	-3.6892	-3.5938	-3.8489
Site 2	-3.7302	-3.6863	-3.5181	-3.7487

Fig. S1 Two preferred binding sites of NP-CH_3 (a), NP-OH (b), NP-COO^- (c), and NP-NH_3^+ (d) on the Fn-$III_{7\text{-}10}$ segments. The bottom shows the docking score reflecting the binding affinity of different NPs to Fn-$III_{7\text{-}10}$.

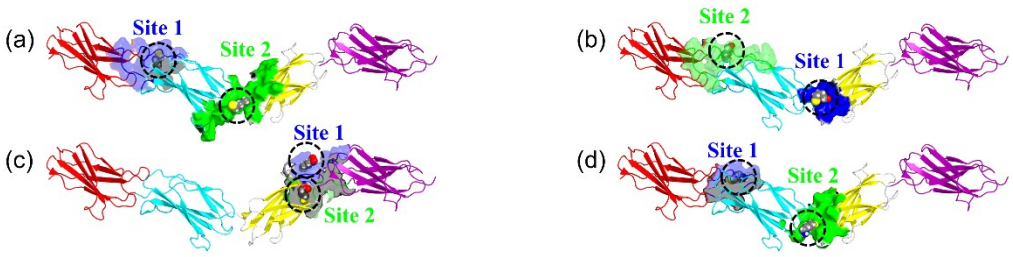

Mode	NP-CH_3	NP-OH	NP-COO^-	NP-NH_3^+
Site 1	-3.9412	-3.6950	-3.8907	-3.8522
Site 2	-3.8162	-3.6793	-3.2142	-3.8092

Fig. S2 Two preferred binding sites of NP-CH_3 (a), NP-OH (b), NP-COO^- (c), and NP-NH_3^+ (d) on the Fn-III_{7B89} segments. The bottom shows the docking score reflecting the binding affinity of different NPs to Fn-III_{7B89}.

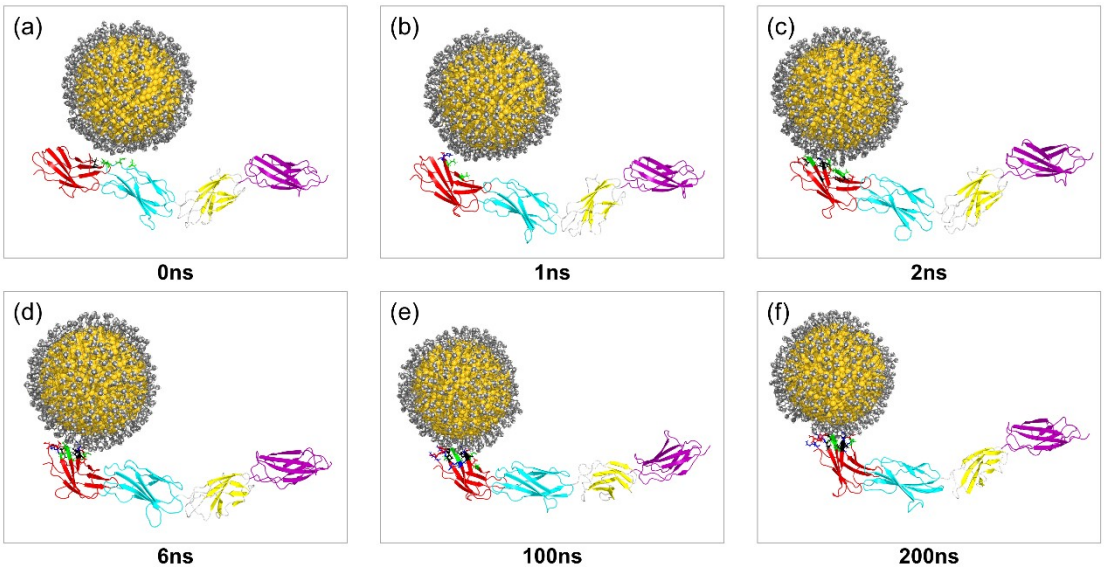

Fig. S3 Time sequence of typical snapshots depicting transfer of NP-CH_3 toward terminal of the Fn-III_{7B89} segment, which is regarded as invalid because Fn-III_{7B89} is an intermediate segment with both terminals connected with other domains.

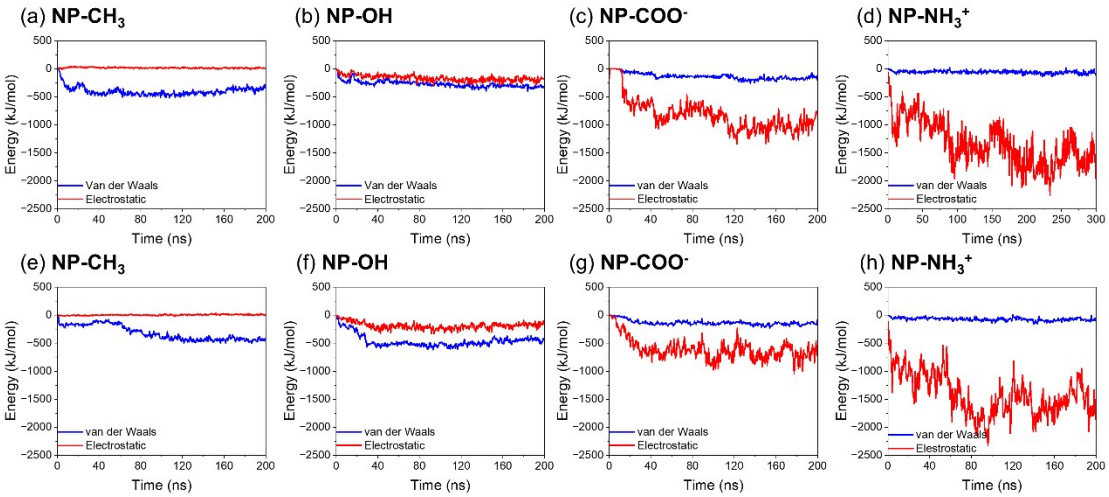

Fig. S4 Time evolutions of the interaction energies between different NPs and two protein segments. (a) NP-CH_3 on Fn-$III_{7\text{-}10}$; (b) NP-OH on Fn-$III_{7\text{-}10}$; (c) NP-COO^- on Fn-$III_{7\text{-}10}$; (d) NP-NH_3^+ on Fn-$III_{7\text{-}10}$; (e) NP-CH_3 on Fn-III_{7B89}; (f) NP-OH on Fn-III_{7B89}; (g) NP-COO^- on Fn-III_{7B89}; (h) NP-NH_3^+ on Fn-III_{7B89}.

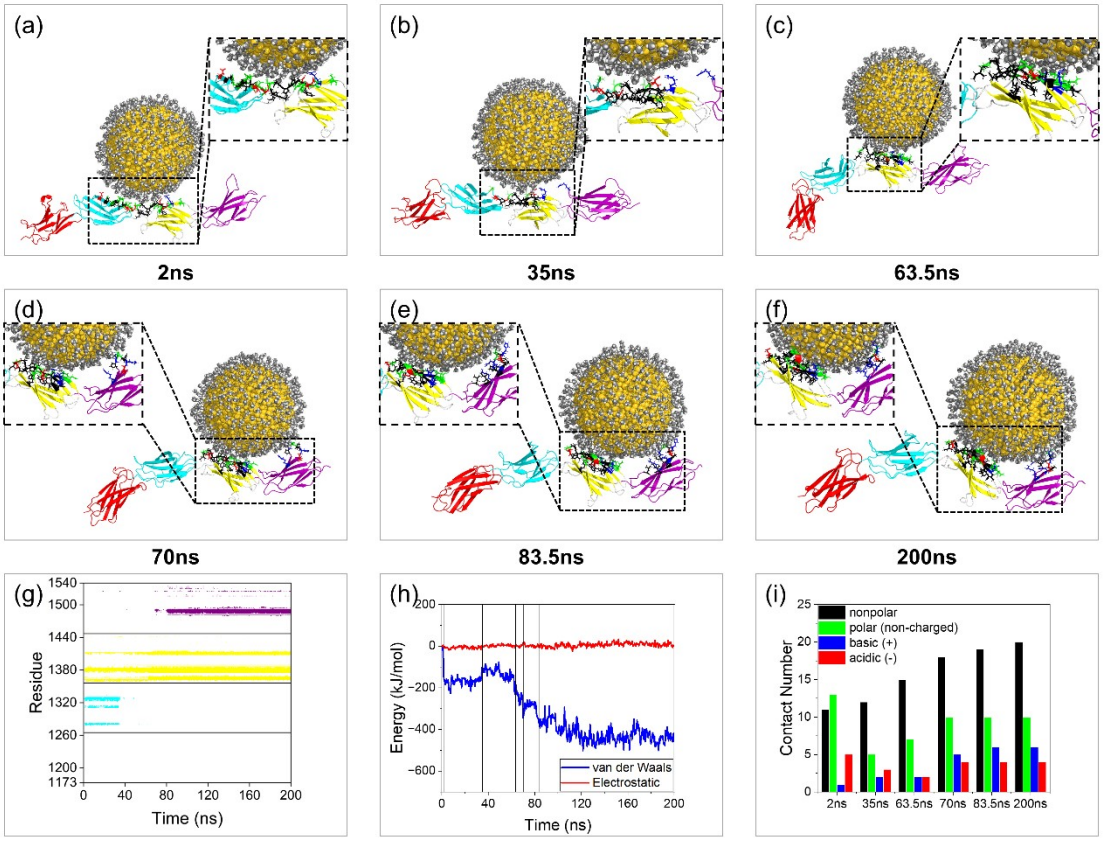

Fig. S5 Migration of NP-CH_3 on the Fn-III_{7B89} segment. (a-f) Time sequence of typical snapshots. (g) Time evolutions of residues in contact with the NP-CH_3. As is seen, NP-CH_3 firstly acquired contacts with residues in domains Fn-III_B and Fn-III_8. At t = 38 ns, it lost contacts with Fn-III_B and acquire more favorable contacts with residues in the domain Fn-III_9. (h) Time evolutions of the van der Waals and electrostatic interaction energies between NP-CH_3 and Fn-III_{7B89}. (i) The numbers of residues of different types in contact with NP-CH_3 at different time points.

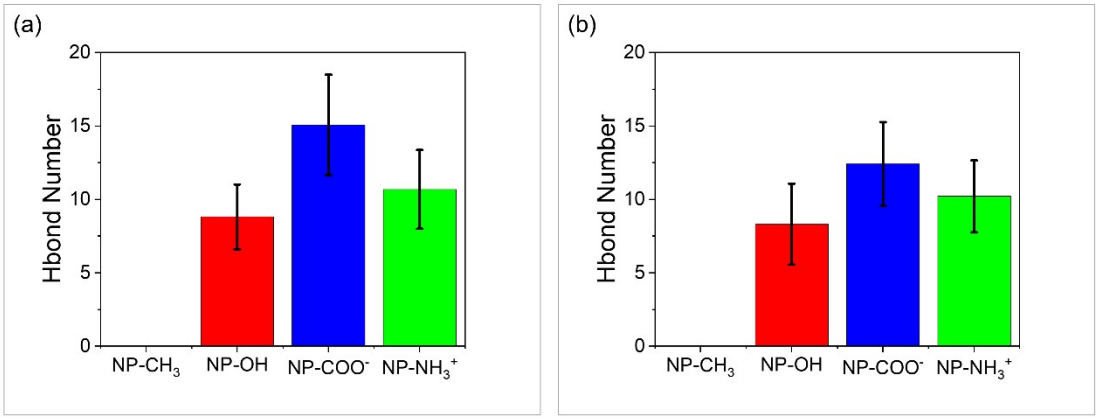

Fig. S6 The numbers of hydrogen bonds formed between different NPs and two protein segments. (a) Fn-III$_{7\text{-}10}$, (b) Fn-III$_{7B89}$.

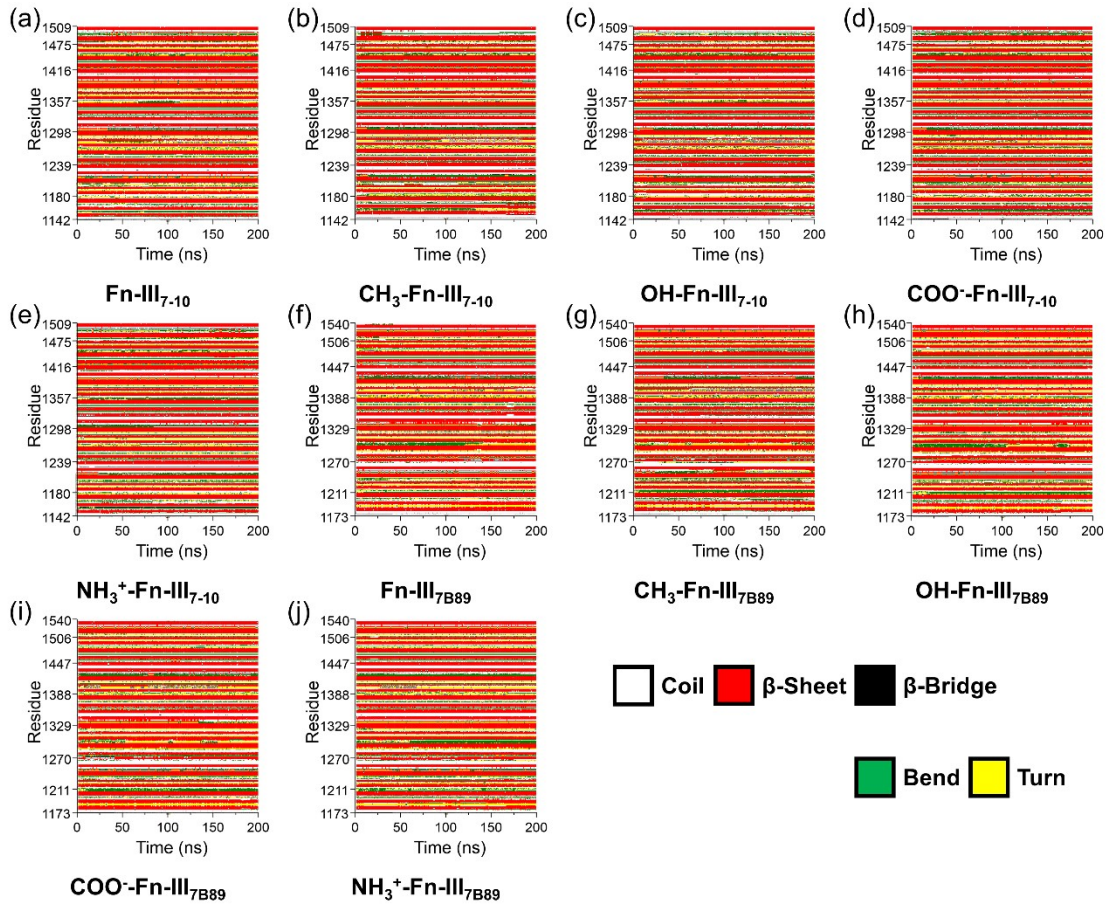

Fig. S7 Time evolutions of the secondary structures of Fn-$III_{7\text{-}10}$ (a-e) and Fn-III_{7B89} (f-j) before (a, f) and after interactions with NP-CH_3 (b, g), NP-OH (c, h), NP-COO^- (d, i), and NP-NH_3^+ (e, j)

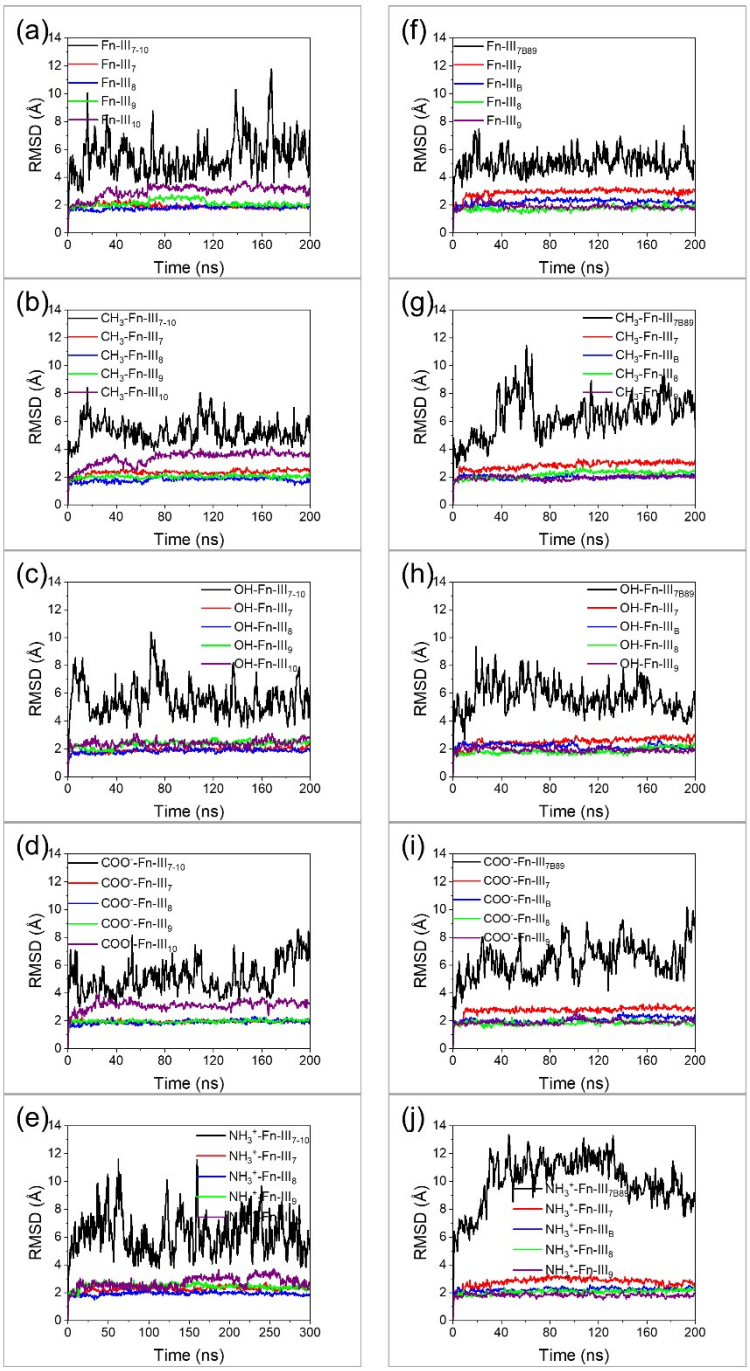

Fig. S8 Time evolutions of the root-mean-square displacement (RMSD) for the entire Fn-III$_{7\text{-}10}$ (a-e) and Fn-III$_{7B89}$ (f-j) segments and different domains before (a, f) and after interactions with NP-CH_3 (b, g), NP-OH (c, h), NP-COO^- (d, i), and NP-NH_3^+ (e, j).

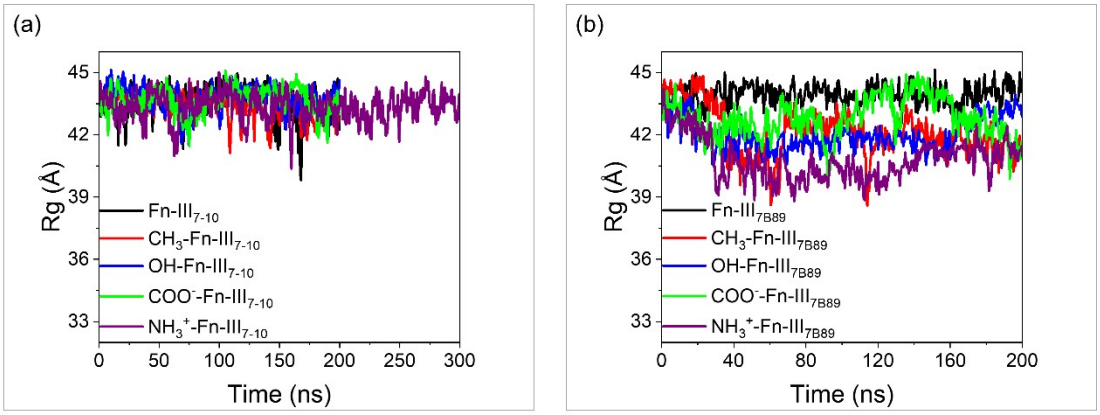

Fig. S9 Time evolutions of the gyration radius (Rg) of Fn-$III_{7\text{-}10}$ (a) and Fn-III_{7B89} (b) segments before and after interactions with different NPs.

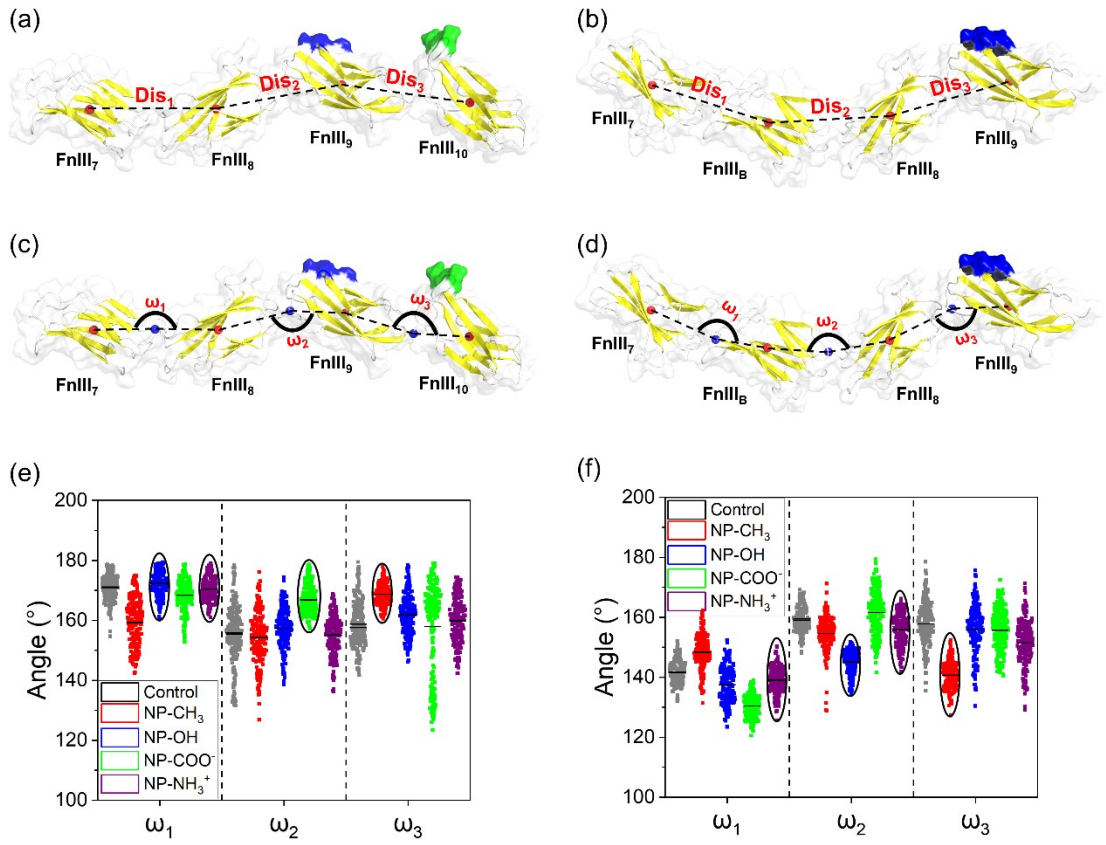

Fig. S10 Protein deformation induced by different NPs. (a-d) Illustration of the calculation of the inter-domain distance (a, b) and angle (c, d). (e, f) The distributions of angles between adjacent domains in Fn-III$_{7\text{-}10}$ (e) and Fn-III$_{7B89}$ (f) segments before and after interactions with different NPs.

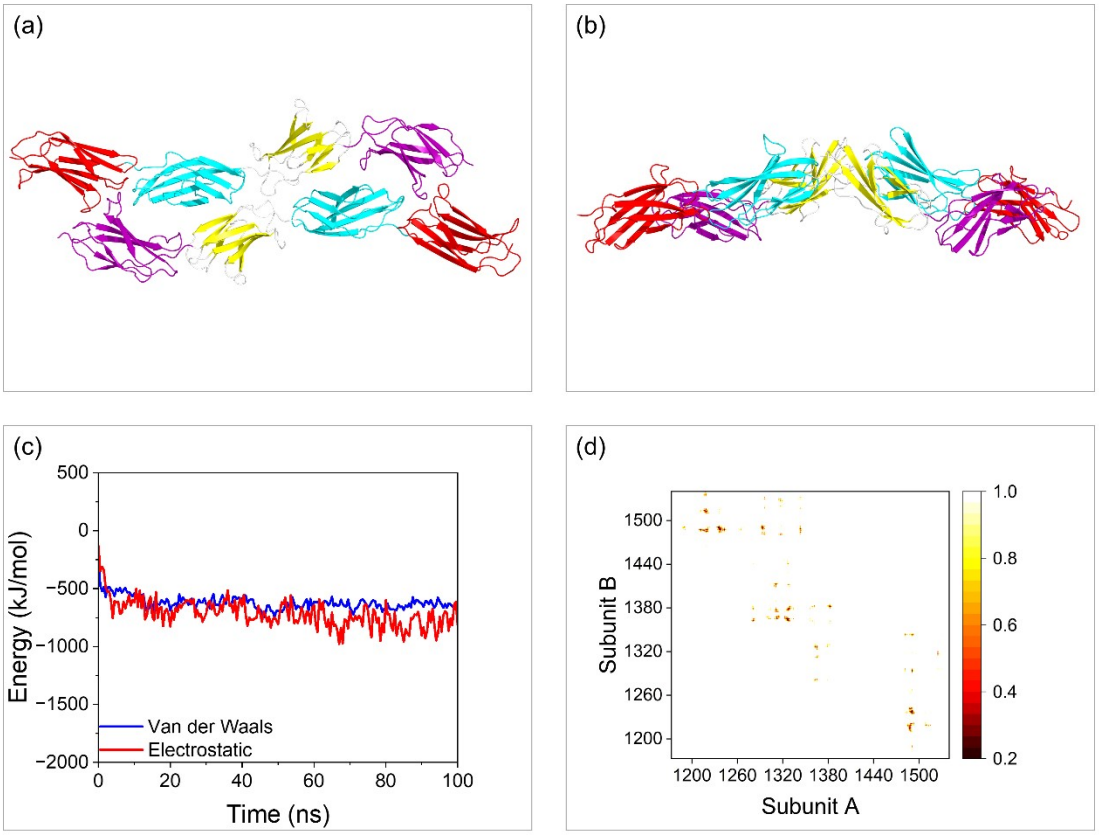

Fig. S11 Dimerization of Fn-III$_{7B89}$. (a, b) Equilibrium structure of the dimerized Fn-III$_{7B89}$ from top (a) and side (b) views. (c) Time evolutions of the interaction energy between two dimerized proteins. (d) The map of probability of inter-subunit residue contacts at the dimer interface of Fn-III$_{7B89}$.

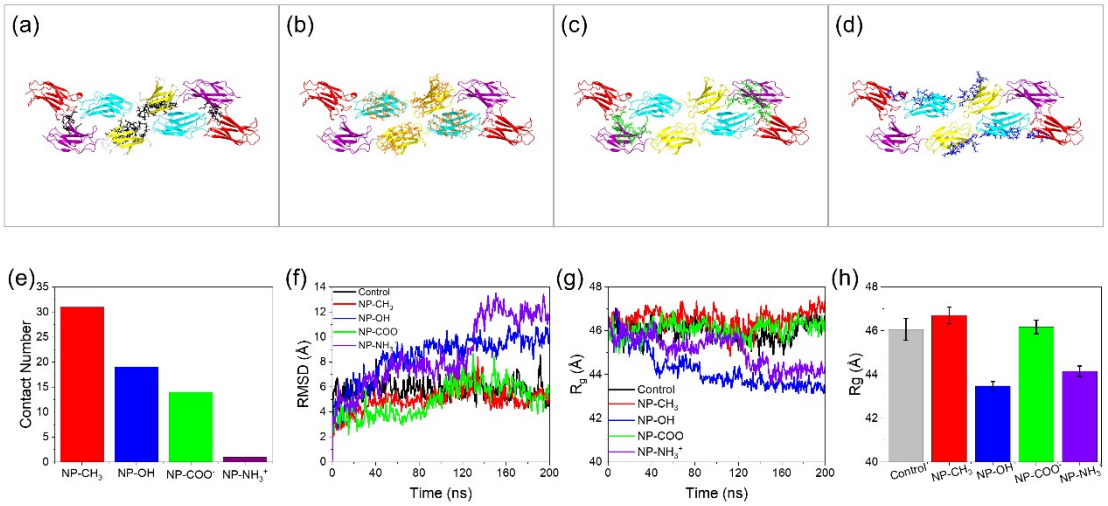

Fig. S12 Perturbation of the Fn-III$_{7B89}$ dimerization by different NPs. (a-d) The equilibrium structures of the Fn-III$_{7B89}$ dimer. Resides in contact with NP-CH_3 (a), NP-OH (b), NP-COO^- (c), and NP-NH_3^+ (d) identified from monomer simulations are displayed with stick models. (e) The number of residues at the dimer interface of Fn-III$_{7B89}$ in contact with different NPs in monomer simulations. (f) Time evolutions of the RMSD of the Fn-III$_{7B89}$ dimer before and after interactions with different NPs. (g) Time evolutions of the Rg of the Fn-III$_{7B89}$ dimer before and after interactions with different NPs. (h) The average Rg of the dimerized Fn-III$_{7B89}$ before and after interactions with different NPs.

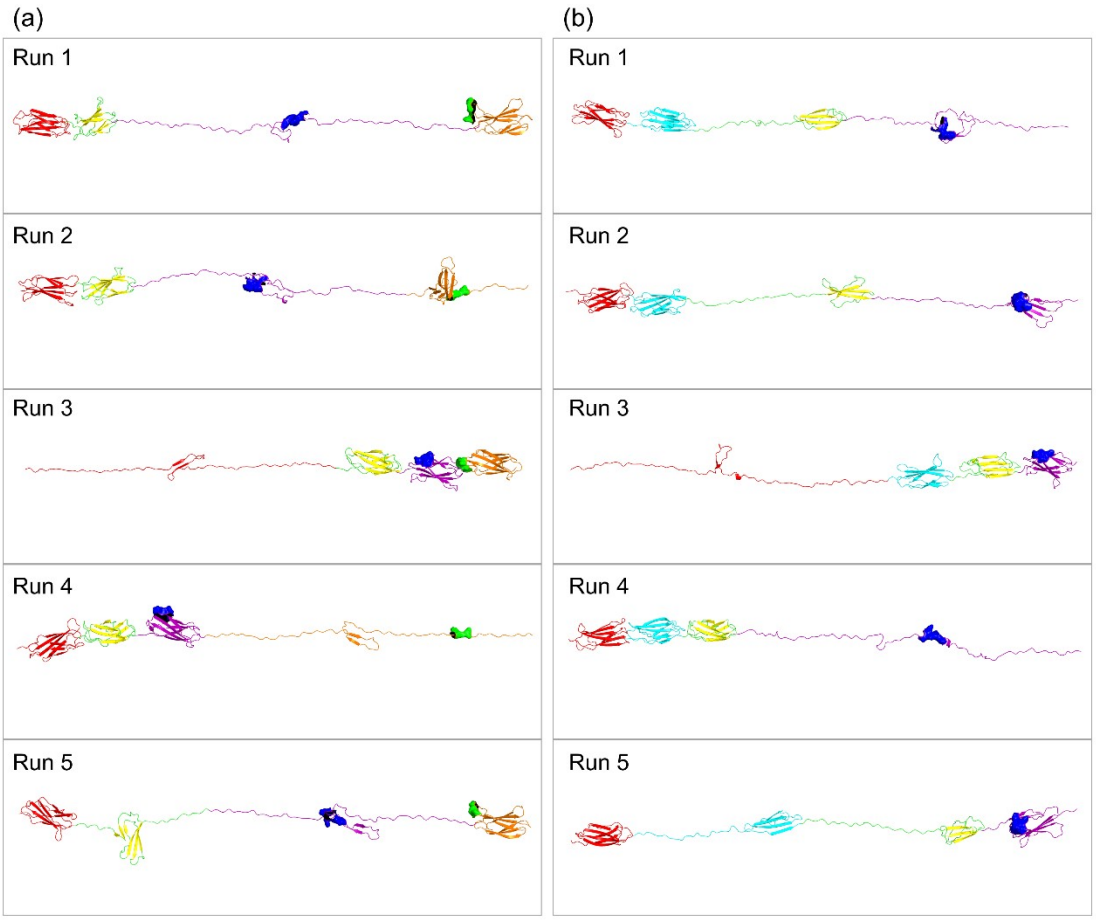

Fig. S13 Final snapshots of five independent simulations of the mechanical stretching on Fn-III$_{7\text{-}10}$ (a) and Fn-III$_{7B89}$ (b).

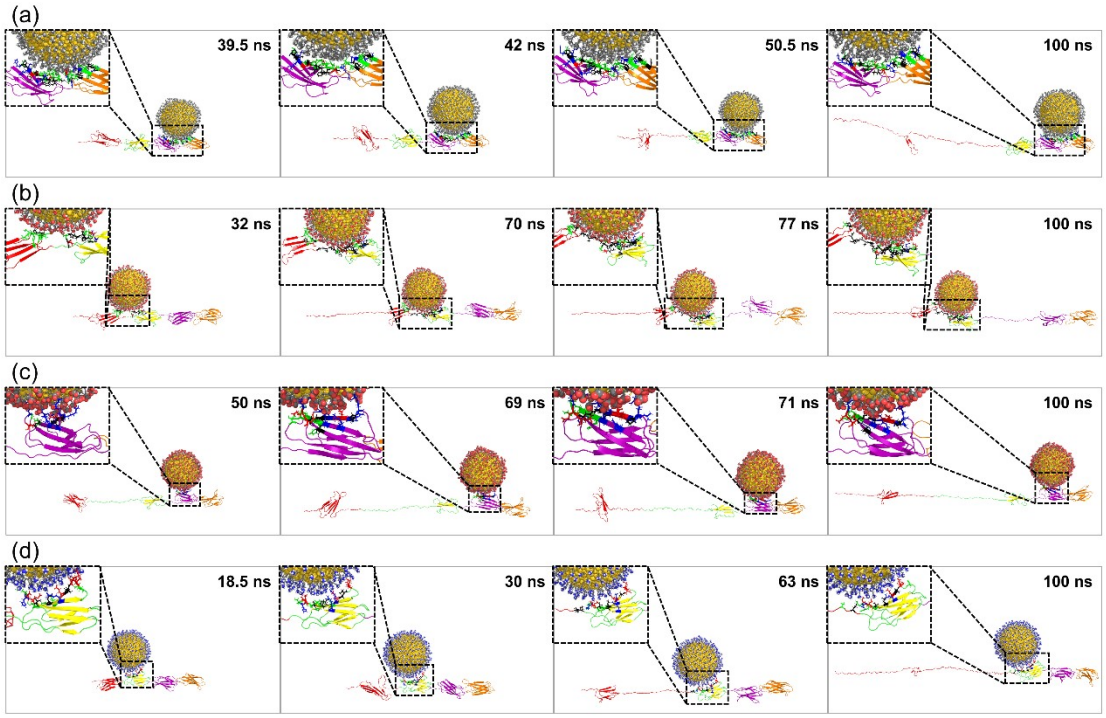

Fig. S14 Time sequences of typical snapshots depicting the mechanical stretching of Fn-III$_{7\text{-}10}$ bound with NP-CH_3 (a), NP-OH (b), NP-COO^- (c), and NP-NH_3^+ (d).

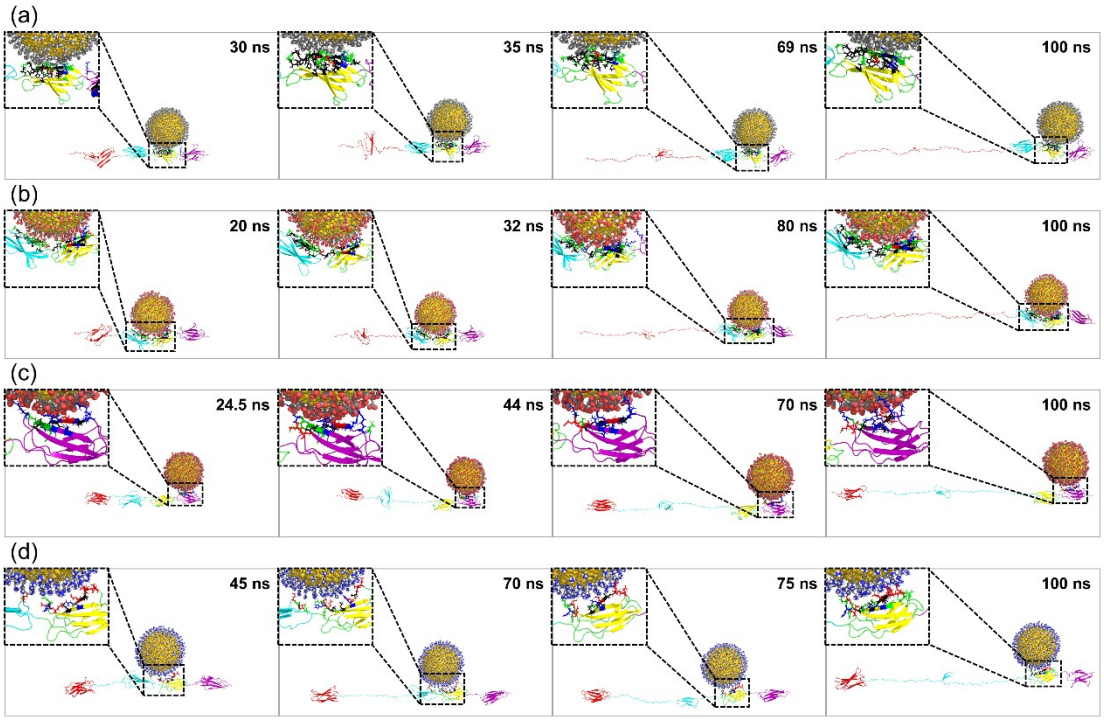

Fig. S15 Time sequences of typical snapshots depicting the mechanical stretching of Fn-III$_{7B89}$ bound with NP-CH_3 (a), NP-OH (b), NP-COO^- (c), and NP-NH_3^+ (d).

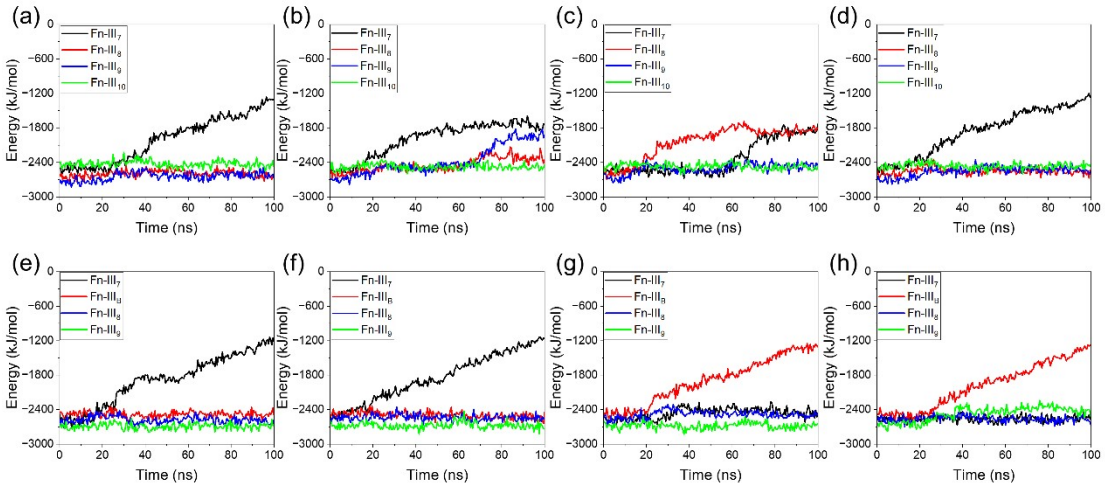

Fig. S16 Time evolutions of the intra-domain interactions in stretched Fn-$III_{7\text{-}10}$ (a-d) and Fn-III_{7B89} (e-h) bound with NP-CH_3 (a, e), NP-OH (b, f), NP-COO^- (c, g), and NP-NH_3^+ (d, h).